Agricultural and Environmental Chemistry

Design, Synthesis, and Herbicidal Activity of Pyrimidine -Biphenyl Hybrids as Novel Acetohydroxyacid Synthase Inhibitors

Ke-Jian Li, Ren-Yu Qu, Yu-Chao Liu, Jing-Fang Yang, ponnam devendar, Qiong Chen, Cong-Wei Niu, Zhen Xi, and Guang-Fu Yang

J. Agric. Food Chem., **Just Accepted Manuscript** • DOI: 10.1021/acs.jafc.8b00665 • Publication Date (Web): 05 Apr 2018

Design, Synthesis, and Herbicidal Activity of Pyrimidine−Biphenyl Hybrids as Novel Acetohydroxyacid Synthase Inhibitors

Ke-Jian Li,[†] Ren-Yu Qu,[†] Yu-Chao Liu,[†] Jing-Fang Yang,[†] Ponnam Devendar,[†] Qiong Chen,[†] Cong-Wei Niu,[‡] Zhen Xi,[‡,#*] and Guang-Fu Yang[†,#*]

[†]*Key Laboratory of Pesticide & Chemical Biology of Ministry of Education, College of Chemistry, Central China Normal University (CCNU), Wuhan 430079, PR China*

[‡]*State Key Laboratory of Elemento-Organic Chemistry, Nankai University (NKU), Tianjin 300071, PR China*

[#]*Collaborative Innovation Center of Chemical Science and Engineering, Tianjin 30071, PR China*

***Corresponding Authors:**

Tel: +86-27-67867800, Fax: +86-27-67867141, E-mail: gfyang@mail.ccnu.edu.cn, zhenxi@nankai.edu.cn.

ABSTRACT: The issue of weed resistance to acetohydroxyacid synthase (EC 2.2.1.6, AHAS) inhibitors has become one of the largest obstacles for the application of this class of herbicides. In a continuing effort to discover novel AHAS inhibitors to overcome weed resistance, a series of pyrimidine−biphenyl hybrids (**4aa**−**bb** and **5aa**−**ah**) were designed and synthesized via a scaffold hopping strategy. Among these derivatives, compounds **4aa** (K_i = 0.09 μM) and **4bb** (K_i = 0.02 μM) displayed higher inhibitory activities against *Arabidopsis thaliana* AHAS than those of the controls bispyribac (K_i = 0.54 μM) and flumetsulam (K_i = 0.38 μM). Remarkably, compounds **4aa**, **4bb**, **5ah**, and **5ag** exhibited excellent post-emergence herbicidal activity and a broad spectrum of weed control at application rates of 37.5−150 g of active ingredient (ai)/ha. Furthermore, **4aa** and **4bb** showed higher herbicidal activity against AHAS inhibitor-resistant *Descurainia sophia*, *Ammannia arenaria* and the corresponding sensitive weeds than that of bispyribac at 0.94−0.235 g ai/ha. Therefore, the pyrimidine−biphenyl motif and lead compounds **4aa** and **4bb** have great potential for the discovery of novel AHAS inhibitors to combat AHAS-inhibiting herbicide-resistant weeds.

KEYWORDS: acetohydroxyacid synthase, herbicide, weed resistance, pyrimidine−biphenyl, structure-based design

INTRODUCTION

With the emergence of various field problems, weed management is still a challenge for researchers, and continuous innovation is essential to maintain the effectiveness of weed management.[1-3] Among the herbicides classified by the Herbicide Resistance Action Committee (HRAC), acetohydroxyacid synthase (AHAS)-inhibiting herbicides have extensive applications for controlling many weed species, and their discovery has been a popular research topic in the herbicide field. AHAS, an important enzyme in the biosynthesis of branched-chain amino acids (BCAAs), catalyzes the conversion of 2-ketobutyrate and pyruvate to 2-aceto-2-hydroxybutyrate and the conversion of two molecules of pyruvate to 2-acetolactate. In plants, BCAAs (isoleucine, leucine and valine) can promote protein synthesis and have an influence on normal plant growth. AHAS inhibitors exert their biological activities by interrupting the above mentioned biosynthetic pathways.[4-7] AHAS-inhibiting herbicides possess a range of advantages, such as excellent crop selectivity, low application rate, benign environmental effects, and low toxicity for mammals.[8] However, the long-term overuse of AHAS-inhibiting herbicides has resulted in the development of serious weed resistance in agricultural applications, and the reports of weeds that are resistant to these herbicides have been gradually increasing in the past decade globally.[9-15] For example, AHAS-inhibiting herbicide-resistant populations of *Descurainia sophia*, *Lindernia micrantha,* *Ammannia arenaria,* and *Monochoria korsakowii,* among others, have been found around the world over the past few years.[16-18] Thus, there is a high demand to develop new AHAS-inhibiting herbicides with higher potency and better anti-resistance properties to control resistant weeds.

To date, extensive studies have been conducted to develop new inhibitors targeting AHAS; however, reports of AHAS inhibitors effectively controlling both AHAS inhibiting herbicide-sensitive weeds and AHAS herbicide-resistant weeds are quite rare.[19-24] Hence, it is necessary to design a novel AHAS inhibitor that not only displays a broader spectrum of weed control but also overcomes the weed resistance to a certain degree. In the past decade, our group has engaged in the design and development of novel AHAS inhibitors.[25-28] We discovered that conformational flexibility in AHAS inhibitors could improve their anti-resistance properties to overcome weed resistance against commercial AHAS-inhibiting herbicides.[29-31] Recently, we reported a series of conformationally flexible triazolopyrimidine-salicylate derivatives with high potency toward *Arabidopsis thaliana* (*At*)AHAS; unfortunately, most of the inhibitors did not exhibit potent herbicidal activity against either AHAS-inhibiting herbicide-resistant weeds or the corresponding sensitive weeds.[29] Thus, it is essential to perform extensive structural modifications of the triazolopyrimidine-salicylate motif to discover more promising AHAS inhibitors.

In this context, scaffold hopping is an effective drug design methodology that has been widely applied to the discovery of potential agrochemicals. It is beneficial to find a novel structure that has an improved inhibitory activity and to identify the pharmacological properties of known activities.[32-35] Interestingly, pyrimidine is an important chemical motif and structural unit of natural products, and its various derivatives are responsible for a broad spectrum of biological activities.[36, 37] Moreover, there are numerous examples of pyrimidine moieties in the substructure of commercial herbicides (including some AHAS inhibitors), fungicides, and insecticides.[38, 39] Therefore, we considered the pyrimidine ring is a promising

replacement for the triazolopyrimidine ring of the triazolopyrimidine–salicylate motif via scaffold hopping and then designed a series of novel pyrimidine–biphenyl hybrids (**4** and **5**) connected by a flexible oxygen linker (Figure 1). Furthermore, the results of computational simulations revealed that the triazolopyrimidine ring (represented by **A**) and the pyrimidine ring (represented by **4aa**) forming similar π–π stacking interactions with amino acid residue W574 in the active pocket of *At*AHAS. Herein, we report the synthesis, *At*AHAS inhibition, herbicidal activity, anti-resistance properties and structure–activity relationships (SAR) of pyrimidine−biphenyl hybrids.

MATERIALS AND METHODS

Chemicals, Instruments and Procedures. All reagents, catalysts, and extra-dry solvents were purchased from commercial suppliers (Sigma-Aldrich, TCI, Merck, J&K, and Aladdin Chemicals). All reactions were monitored using thin-layer chromatography (TLC) run on silica gel glass plates (Qingdao Broadchem Industrial, Qingdao, China). Melting points were recorded on a model B-545 melting point apparatus (Büchi, Flawil, Switzerland), and the values were uncorrected. ^{1}H NMR and ^{13}C NMR spectra were recorded using a Mercury-Plus 600 or 400 spectrometer (Varian Inc., Palo Alto, CA) with temperature control at 21−23 °C using DMSO-d_6 or $CDCl_3$ as the solvent and tetramethylsilane (TMS) as the internal reference. In the spectra, the chemical shifts (δ) were given in parts per million (ppm). Mass spectrometry (MS) data were obtained with a DSQ II GC-MS (Thermo Fisher, Austin, TX) instrument with an electrospray ionization (ESI) source. High-resolution mass spectra (HRMS) were determined with a model 6224 time-of-flight liquid chromatograph–mass spectrometer

106 equipped with a 250 mm × 4.6 mm i.d., 5 μm, Eclipse XDB-C18 column (Agilent
107 Technologies, Santa Clara, CA).

108 *Synthesis of Compound **2*** (Figure 2). A catalytic amount of $Na_2WO_4 \cdot 2H_2O$ was added to
109 a stirred mixture of compound **1** (0.10 mol) and 100 mL of acetic acid at 25 °C. Next, 30%
110 H_2O_2 (0.11 mol) solution was added slowly at −10 °C with continued vigorous stirring. The
111 system temperature was maintained at 70 °C for an additional 5 h. After cooling to 0 °C, the
112 reaction was quenched with 200 mL of aqueous Na_2SO_3 solution. The resulting solid was
113 collected by filtration, washed with cold water (3×30 mL), and dried in a vacuum desiccator
114 at 60 °C to afford compound **2** as an off-white solid (19.4 g, yield 89%): ^{1}H NMR (600 MHz,
115 DMSO-d_6) δ 6.57 (s, 1H), 4.00 (s, 3H), 3.40 (s, 6H). EIMS: m/z = 218.11 (M^+).

116 *General Procedure for the Synthesis of **4aa**−**bb*** (Figure 2). The key intermediate 6-aryl
117 salicylic acid derivatives (**3**) were synthesized according to our previous reports.[40-42] In a 100
118 mL flask, the derivatives **3** (2.0 mmol) were dissolved in 20 mL of toluene. Then, anhydrous
119 K_2CO_3 (8.0 mmol) was slowly added to the reaction mixture with stirring at room temperature.
120 After 1 h, compound **2** (2.1 mmol) was added to the reaction mixture, the whole system was
121 put into a preheated oil bath (120 °C), and the reaction progress was monitored by TLC until
122 the reaction was complete. After cooling to room temperature, the reaction was quenched with
123 aqueous HCl (0.5 N, 30 mL) and extracted with EtOAc (3×15 mL). The combined organic
124 layers were dried over anhydrous Na_2SO_4 and concentrated under vacuum. The residue was
125 purified via flash column chromatography (*n*-hexane/acetone = 20:8) to provide target
126 compounds **4aa**−**bb** (yields 32−85%).

General Procedure for the Synthesis of ***5aa*****−*****ah*** (Figure 2). In a 25 mL flask, compound **4aa** or **4bb** (1.0 mmol) and Cs_2CO_3 (1.1 mmol) were dissolved in 5 mL of *N,N*-dimethylformamide (DMF). After stirring at room temperature for 10 min, the corresponding alkyl halide (1.50 mmol) was added to the reaction mixture. The temperature of the reaction solution was increased to 50 °C and maintained for 2 h. After completion of the reaction as monitored by TLC, the reaction mixture was quenched with 20 mL of water, and the mixture was extracted with EtOAc (3×5 mL). The combined organic layers were dried over anhydrous Na_2SO_4 and concentrated under vacuum. The residue was purified via flash column chromatography (*n*-hexane/EtOAc = 20:4) to afford title compounds **5aa**−**af** (yields 80−94%).

General Procedure for the Synthesis of ***5ag*** *and* ***5ah*** (Figure 2). In a single-neck round-bottomed flask, compound **4aa** or **4bb** (1.0 mmol) was dissolved in 10 mL of anhydrous THF. After cooling to 0 °C in an ice bath, NaOH (1.0 mmol) was added to the reaction system. As the reaction proceeded, a white solid was precipitated from the reaction mixture. It was collected by filtration and washed with THF (3×5 mL) to afford compound **5ag** (yield 73%) or compound **5ah** (yield 65%).

X-ray Diffraction. A colorless crystal of compound **4bb** was obtained directly from acetone/*n*-hexane. Its X-ray single-crystal diffraction data were collected on a SMART APEX DUO CCD area detector diffractometer (Bruker AXS, Madison, WI) at 296 K using Mo Kα radiation (λ = 0.71073 Å). All the non-hydrogen atoms of compound **4bb** were refined with anisotropic displacement parameters. The hydrogen atoms were placed and observed in geometrically idealized positions. The integration of the diffraction profiles and the methods

of structural analysis were carried out using SAINT Plus software (Bruker AXS, Madison, WI) and SHELXS97 program (University of Gottingen, Gottingen, Germany), respectively. The crystallographic data for crystal **4bb** were deposited with the Cambridge Crystallographic Data Centre (CCDC) with deposition number 1558576.[43]

***At*AHAS Inhibitory Activity Assay.** The expression and purification of *At*AHAS were performed using the same methods as those described in previous reports.[25-31] The inhibition of *At*AHAS was measured by kinetic parameters (K_i value) between the enzyme and inhibitors. The non-linear least-squares and simplex methods were used to calculate the kinetic parameters by error minimization. The K_i values were calculated by fitting the data to the following equation:

$$v_i = v_\infty + (v_0 - v_\infty)/(1+[I]/K_i^{app})$$

where [I] and K_i^{app} represent the concentration of the prepared inhibitors and apparent inhibition constant (the inhibitor concentration giving 50% inhibition), respectively. v_0 and v_i are the reaction rate in the absence or presence of the inhibitor, respectively. If the initial analysis indicated that the residual activity (v_∞) at a saturating inhibitor concentration is not significantly larger than zero, the data were reanalyzed with $v_\infty = 0$.

Molecular Simulation and Comparative Molecular Field Analysis. The crystal structure of *At*AHAS (PDB ID: 5K2O) was downloaded from the Protein Data Bank.[6] Computational modeling studies of representative compounds were performed using AutoDock 4.2 software, and the parameters of the docking model were programmed to the recommended default values. A total of 265 runs clustered by 2 Å of root-mean-square deviation (RMSD) criteria were launched for each compound. The final binding modes with

reference to the reported co-crystal structure between bispyribac and *At*AHAS were selected by the docking score. PyMOL v1.3 software was used to visualize and analyze the docking results. The binding free energy for each complex was estimated using the molecular mechanics Poisson−Boltzmann surface area (MM-PBSA) method.[44]

On the basis of the best combining conformation, the three-dimensional structures of **4aa**−**4bb** were generated with the default setting of SYBYL 6.9 (Tripos Inc., St. Louis, MO), and the molecules were subjected to energy minimization at a gradient of 1.0 kcal/mol with a delta energy change of 0.05 cal/mol. We calculated the CoMFA descriptors and electrostatic and steric field energies on the condition of the SYBYL default parameters, which included a grid point spacing of 2.0 Å, a minimum σ (column filtering) of 2.0 kcal/mol, an energy cut off of 30.0 kcal/mol, and a sp^3 carbon probe atom with a +1 charge.

Greenhouse Herbicidal Assay. The herbicidal activities were evaluated in the Zhejiang Research Institute of Chemical Industry (Hangzhou, China). All the target compounds (**4aa**−**bb** and **5aa**−**ah**) were dissolved in 100% DMF and then diluted with Tween-80 (concentration: 100 g/L). The resulting solutions were diluted with water to the appropriate concentrations before use. The post-emergence herbicidal activity of the compounds was evaluated against three dicotyledonous weeds, *Brassica juncea* (*B.j.*), *Chenopodium serotinum* (*C.s.*), and *Rumex acetosa* (*R.a.*), and three graminaceous weeds, *Alopecurus aequalis* (*A.a.*), *Polypogon fugax* (*P.f.*), and *Poa annua* (*P.a.*). In addition, *Abutilon theophrasti* (*A.t.*), *Amaranthus retroflexus* (*A.r.*), *Digitaria sanguinalis* (*D.s.*), *Eclipta prostrata* (*E.p.*), and *Echinochloa crusgalli* (*E.c.*) were selected to evaluate the herbicidal spectrum of representative compounds. In a greenhouse, the prepared soil was filled to 3/4 of

193 the height of the flowerpots (with an inner diameter of approximately 7.5 cm). Approximately
194 20 seeds of each tested weed were sown and grown at temperatures alternating from
195 15−30 °C. When these weeds had grown to approximately the three-leaf stage, they were
196 sprayed with a stock solution containing the inhibitors at the required concentrations (g ai/ha).
197 Moreover, mixtures of DMF and Tween-80 were selected as solvent control groups. After 20
198 days of treatment with the inhibitors, the growth inhibition rates were calculated (three
199 duplicates per experiment) according to previously reported methods.[45]

200 *Descurainia sophia* (sensitive *D. Sophia* and resistant *D. Sophia* mediated by AHAS
201 mutation) and *Ammannia arenaria* (sensitive *A. arenaria* and bensulfuron methyl-resistant *A.*
202 *arenaria*) were selected to test the anti-resistance properties of the synthesized compounds.[17]
203 Similar to the above preparation, the seeds of *D. sophia* and *A. arenaria* were treated with
204 0.05% gibberellic acid (GA3), and then dormancy was broken after 24 h. In a phytotron, the
205 seeds were planted in flowerpots, and the growth temperature was maintained at 15−25 °C
206 (day and night). Upon reaching the four-leaf stage, the seedlings were moved to a greenhouse
207 and treated with the selected inhibitors. Furthermore, the post-emergence herbicidal activity
208 of the compounds was visually evaluated after 35 days of treatment, and each experiment was
209 carried out with three replications.
210

211 **RESULTS AND DISCUSSION**

212 **Chemistry.** As shown in Figure 2, target compounds **4aa**−**bb** and **5aa**−**ah** were
213 prepared by using 4,6-dimethoxy-2-(methylthio)pyrimidine, **1**, as a starting material. The
214 oxidation of methyl sulfide, **1**, using 30% H_2O_2/cat. $Na_2WO_4 \cdot 2H_2O$ in AcOH afforded

methyl sulfone, **2**, in good yield. The key intermediate 6-arylsalicylates, **3**, were synthesized via two different synthetic routes (Figures 3A and B) as reported previously.[40-42] When R^1 in compound **3** was a hydrogen or halogen (H, F, Cl), the synthesis occurred in three steps, as shown in method A. When R^2 was a methoxyl or methyl group (OMe, Me), the synthesis occurred in five steps, as outlined in method B. In the subsequent step, methyl sulfone, **2**, was treated with various substituted 6-arylsalicylates, **3**, in the presence of K_2CO_3, resulting in target compounds **4aa**−**bb** (yields 32−85%) via a nucleophilic substitution reaction. To synthesize target compounds **5aa**−**af**, compounds **4aa** and **4bb** were treated with the corresponding alkyl halides in the presence of Cs_2CO_3 in DMF. In addition, compound **4aa** or **4bb** reacted with NaOH in THF, yielding the corresponding sodium salts **5ag** and **5ah**, respectively. The chemical structures of all the synthesized target compounds were identified by ^{1}H NMR, ^{13}C NMR and HRMS analyses. Furthermore, the structure of compound **4aa** was confirmed by single-crystal X-ray diffraction (Figure 4).

AHAS Inhibitory Activity, SAR and CoMFA. From the results of the molecular modeling of compound **4aa** with *At*AHAS (PDB entry 5K2O),[6] we found that it had two evident interactions in the active pocket of *At*AHAS (Figure 1). The pyrimidine ring of compound **4aa** formed a π−π interaction with W574, and the benzoic acid part showed a hydrogen bonding interaction with residues S653, R377, and K256. The analyzed results indicated that the introduction of various substituents into the core skeleton (pyrimidine−biphenyl hybrid) at the R^1 and R^2 positions could increase the interactions with the enzyme. We then synthesized **4ab**−**bb** and systemically investigated the kinetic constants (**(**K_i values) of all the compounds against *At*AHAS. The commercial AHAS-inhibiting

herbicides bispyribac and flumetsulam were selected as the positive controls. As shown in Table 1, most of the synthesized compounds displayed strong inhibitory activities against *At*AHAS, and some of them showed even better potencies than the commercial controls. In particular, among the compounds tested, compounds **4aa** (K_i = 0.09 μM) and **4bb** (K_i = 0.02 μM) displayed the highest enzyme inhibitory activities; comparatively, the K_i values of bispyribac and flumetsulam were 0.54 μM and 0.38 μM, respectively. Moreover, compounds **4am** (K_i = 0.18 μM), **4al** (K_i = 0.25 μM), **4au** (K_i = 0.20 μM), and **4av** (K_i = 0.41 μM) also showed excellent inhibitory activities that were comparable to that of flumetsulam.

On the basis of the observed K_i values of these compounds against *At*AHAS, the major SARs can be revealed. The different aromatic groups at R^1 have a significant impact on activity of the compounds. The results indicated that five-membered furanyl-substituted compounds **4ai** (K_i = 0.66 μM) and **4aj** (K_i = 0.51 μM), and isoxazolyl-substituted compound **4al** (K_i = 3.78 μM) displayed enhanced activity compared to (un)substituted six-membered heterocyclic (pyridyl or pyrimidinyl)-substituted compounds **4ab**−**ah** (K_i range of 4.52−705.00 μM). Furthermore, the compound with a bulky naphthyl group at R^1 (**4al**, K_i = 0.25 μM) showed better potency than those of the heterocyclic-substituted compounds **4ab**−**4aj** and a similar K_i value to that of the controls bispyribac (K_i = 0.54 μM) and flumetsulam (K_i = 0.38 μM). When an unsubstituted phenyl group was introduced at R^1, the resulting compound (**4aa**) displayed excellent activity (K_i = 0.09 μM) compared to compounds **4ab**−**al** substituted with heterocyclic or naphthyl groups at the same position. We further studied the influence of introducing substituted phenyl groups at R^1 on inhibitory activity. As shown in Table 1, the inhibition constants of these compounds (**4am**−**aw**)

appeared in the micromolar to nanomolar range, and some of the compounds showed higher potency than that of the controls. Furthermore, we found that the positions of substituents (*ortho*-, *meta*- and *para*-positions) on the phenyl group significantly affected the *At*AHAS inhibitory activities of the resulting compounds. In most cases, when the phenyl group was monohalogenated, the *para*-substituted compound had higher inhibitory activity than that of the *meta*- and *ortho*-substituted compounds. For example, the fluoro- and chloro-substituted compounds showed the following trend in activity: 4-F (**4ar**) > 2-F (**4ap**) ≈ 3-F (**4aq**); 4-Cl (**4au**) >2-Cl (**4as**) > 3-Cl (**4at**). When different halogens were introduced at the *para*-position of the phenyl group, the chloro-substituted compound demonstrated higher activity than the bromo-substituted compound and much higher activity than the fluoro-substituted compound, i.e., 4-Cl (**4au**) > 4-Br (**4av**) > 4-F (**4ar**). The nature of the substituent at the phenyl group also affected the activity of the compound. For example, when we introduced an electron-donating group, the resulting compound exhibited more potent *At*AHAS inhibitory activity than that of compounds with an electron-withdrawing group, e.g., 4-Me (**4am**) > 4-NO_2 (**4ao**) and 4-OMe (**4an**) > 4-NO_2 (**4ao**). From the above results, the SAR of the *para*-substituted phenyl compounds can be summarized as follows: 4-Me (**4am**) > 4-Cl (**4au**) > 4-Br (**4av**) > 4-F (**4ar**) > 4-OMe (**4an**) > 4-NO_2 (**4ao**).

In addition, we kept R^1 as a phenyl group while simultaneously introducing different substituents at the R^2 position, which had a significant effect on the *At*AHAS inhibitory activity of the resulting compound. For instance, when we replaced the methyl group at R^2 in compound **4aa** with a fluoro (**4az**), chloro (**4ba**) or methoxy (**4ax**) group, we found that these changes were detrimental to the activity of the compound compared with parent **4aa**.

Surprisingly, if we introduced a hydrogen atom in place of methyl group, the activity of the resultant compound (**4bb**, K_i = 0.02 μM) was 4.5 times greater than that of compound **4aa** (K_i = 0.09 μM). To understand the structural basis, we performed molecular modeling on representative compounds **4aa**, **4ax**, **4az**, and **4bb** (R^2 = Me, OMe, F, H, respectively). As depicted in Figures 5A−D, the compounds **4ax**, **4az**, and **4bb** had a similar docking mode to that of compound **4aa**, which was discussed earlier (Figure 1). However, the K_i values of these four compounds showed statistically significant differences. Considering their molecular structures, the main difference was in the R^2 group, indicating that this position might have a significant effect on the binding between the ligand and *At*AHAS. To explain this finding, we further conducted binding free energy calculation and compared the binding conformations among the different compounds. The results (Table 2) revealed that the van der Waals (VDW) interaction of compound **4aa** was enhanced compared with that of **4bb** ($\Delta\Delta E_{VDW} = \Delta E_{VDW,4aa} - \Delta E_{VDW,4bb} = -1.81$ kcal/mol). However, the number of rotatable bonds in **4aa** (R^2 = Me) decreased compared with that of **4bb** (R^2 = H) because of the increased steric hindrance in the active pocket, which caused an obvious increase in entropy compensation ($-T\Delta\Delta S$ = 4.08 kcal/mol). By integrating the energy, compound **4bb** showed a better binding affinity with *At*AHAS than that of compound **4aa** ($\Delta\Delta G_{Cal} = \Delta G_{Cal,4aa} - \Delta G_{Cal,4bb}$ = 1.68 kcal/mol). When analyzing the binding modes of compounds **4ax** and **4bb** (Figure 5B, D), we observed that the binding conformation of **4ax** was offset upward compared with that of **4bb** because the OMe group of **4ax** displayed steric repulsion with residue S168. This repulsion resulted in weakened hydrogen bonding between the ligand and amino acid residues S653 and K256. From the perspective of the binding free energy (Table

2), the increased distance caused a dramatic reduction in the electrostatic energy of **4ax** relative to that of compound **4bb** ($\Delta\Delta E_{ELE} = \Delta E_{ELE,4ax} - \Delta E_{ELE,4bb}$ = 16.96 kcal/mol). Additionally, the VDW energy and entropy of compound **4ax** (R^2 = OMe) were increased over those of compound **4bb** (R^2 = H) due to the introduction of a substituent group at R^2. Overall, the energy component analysis indicates that the binding free energy of **4az** with *At*AHAS is lower than that of **4bb** ($\Delta\Delta G_{Cal} = \Delta G_{Cal,4az} - \Delta G_{Cal,4bb}$ = 4.06 kcal/mol). The binding free energy of the fluoro-substituted compound (**4az**) was the lowest among the four representative compounds. A possible reason for this finding is that the fluorine atom causes the molecule to be more electronegative, which may induce electrostatic repulsion with negatively charged residue D376 (Figure 5C). According to the above energy component analysis and the binding mode comparison, compounds **4aa** and **4bb** could be better *At*AHAS inhibitors.

To further understand the relationship between the substituents and *At*AHAS inhibition, a brief comparative molecular field analysis (CoMFA) of 27 representative compounds **4aa**−**bb** was performed. As shown in Figure 6, a linear correlation between the experimental and calculated *At*AHAS inhibitory activities (pK_i) was acquired with a correlation coefficient (R^2) of 0.933, which confirmed the reliability of the theoretical models constructed in this work. The predicted CoMFA model of this series collected for the training set was statistically significant with a cross-validated coefficient (q^2) of 0.752, a conventional coefficient (r^2) of 0.935, and a predicted correlation coefficient (r^2 pred) of 0.919. The electrostatic contour map is shown in the blue and red highlighted areas (Figure 7A). The contour plot of the steric contributions is shown in the yellow and green

highlighted regions in Figure 7B. The yellow polyhedra show that introducing a bulky group in this position negatively affects the *At*AHAS inhibitory of these compounds. For example, compound **4bb** (R^2 = H, K_i = 0.02 μM) is a more potent inhibitor than **4ax** (R^2 = OMe, K_i = 26.80 μM) against *At*AHAS, even though they have the same R^1 group (R^1 = Ph). A similar phenomenon was also displayed by compounds **4aa** and **4ax** and compounds **4au** and **4ay**. In addition, the green positions denote where a sterically bulky group would be beneficial for *in vitro At*AHAS inhibition. Above all, these rules further illuminated the molecular mechanism of the SAR.

Herbicidal Activity and SAR. The post-emergence herbicidal activity of title compounds **4aa**−**bb** and **5aa**−**ah** was evaluated against six kinds of representative weeds, *B.j.*, *C.s.*, *R.a.*, *A.a.*, *P.f.*, and *P.a.*, under greenhouse conditions. The AHAS-inhibiting herbicides flumetsulam and bispyribac were selected as positive controls, and the herbicidal activity results are shown in Table 1. In most cases, the weed inhibition of these compounds was consistent with their *in vitro* results. When applied at a rate of 150 g ai/ha, several compounds showed greater than 60% weed control against some of the tested weeds, and **4am** and **4aq** displayed 70−100% inhibition against five of the six tested weeds. Very promisingly, **4aa**, **4bb**, **5ag**, and **5ah** exhibited a weed control spectrum (inhibition >80%) that was broader than or equivalent to that of the commercial herbicides flumetsulam and bispyribac at the same dosage.

As shown in Table 1, most of the heterocyclic- or naphthyl-substituted (at R^1) compounds (**4ab**−**al**) did not show promising herbicidal activity. Only compounds **4ab**, **4ac**, **4ad**, and **4af** exhibited over 80% inhibition against one or two of the tested weeds (*B.j.*/*A.a.*).

347 The introduction of the (un)substituted phenyl group at R^1 was favorable to the herbicidal
348 activity compared to the activity of compounds **4ab**−**al**. Notably, compound **4aa** with the
349 phenyl group at R^1 displayed >80% inhibition against the three tested dicotyledonous weeds
350 (*B.j.*/*C.s.*/*R.a.*) and even had 90% control against the three graminaceous weeds
351 (*A.a.*/*P.f.*/*P.a.*). Furthermore, we observed a clear SAR when introducing the substituted
352 phenyl at R^1 (**4am**−**aw**). For example, compounds featuring a phenyl ring substituted with an
353 electron-withdrawing group (**4am**, 4-NO_2-Ph) displayed lower herbicidal activity than those
354 featuring a phenyl ring substituted with an electron-donating group (**4am**, 4-Me-Ph; **4an**,
355 4-OMe-Ph). When a halogen-substituted phenyl was introduced at R^1, the SAR was
356 summarized as follows (with a few exceptions against some of the tested weeds): (i) *p*-Cl
357 (**4au**) > *p*-Br (**4av**) > *p*-F (**4ar**), (ii) *p*-F (**4ar**) > *m*-F (**4aq**) > *o*-F (**4ap**) and (iii) *p*-Cl (**4au**) >
358 *m*-Cl (**4at**) > *o*-Cl (**4as**).

359 The introduction of substituents at the R^2 position also had a significant influence on the
360 herbicidal activity. As shown in Table 1, compound **4bb** (R^2 = H) exhibited greater than 80%
361 control against the six tested weeds, which was comparable to that of compound **4aa** (R^2 = Me)
362 at 150 g ai/ha. However, compounds bearing fluoro, chloro and methoxy groups at the R^2
363 position (**4ax**−**ba**) lost their herbicidal activity (except compound **4ba** against *B.j.*) against all
364 the weeds at the tested application rate. These results were consistent with the *At*AHAS
365 inhibitory activity of these compounds.

366 It is well known that pro-drugs can improve the absorption, distribution, metabolism, and
367 excretion (ADME) properties of a compund.[46] In this work, the carboxyl group in the core
368 structure was regarded as a good modification site to design a pro-drug. We synthesized

369 another set of R^3-substituted compounds (**5aa**−**ah**) based on compounds **4aa** and **4bb** and
370 examined the effect of R^3 substitution on herbicidal activity. Steric factors had a significant
371 impact on herbicidal activity. Compound **5aa** (R^3 = Me) showed moderate control (30−50%)
372 against four different weeds (*B.j.*/*R.a.*/*A.a.*/*P.f.*) at 150 g ai/ha. However, compounds **5ab** (R^3
373 = Et), **5ad** (R^3 = CH_2COOMe), **5ae** (R^3 = CH_2COOEt), and **5af** (R^3 = $CHCH_3COOMe$) with
374 sterically larger substituents at R^3 (compared to **5aa**) displayed poor herbicidal activities
375 against all the tested weeds. Compounds **5aa** (R^2 = Me, R^3 = Me) and **5ac** (R^2 = H, R^3 = Me)
376 had dramatically decreased herbicidal activities relative to their parent compounds **4aa** and
377 **4bb**, respectively. These results implied that introduction of the ester group (pro-drug) had a
378 detrimental effect on herbicidal activity. A conceivable explanation for the poor *in vivo*
379 activity of **5aa**−**af** is that the ester group exerts a large steric hindrance effect because of its
380 *ortho* substituents, which could make the ester-containing group difficult for plants to
381 hydrolyze. However, carboxylic acid sodium salts **5ag** and **5ah** displayed equivalent
382 herbicidal activity to that of carboxylic acids **4aa** and **4bb**.

383 **Herbicidal Spectrum and Anti-resistance Properties against Resistant Weeds.** Based
384 on the herbicidal activity results, we selected four promising compounds, **4aa**, **4bb**, **5ag**, and
385 **5ah**, to evaluate their herbicidal activity against more weed biotypes (11 kinds) at application
386 rates of 37.5−150 g ai/ha. As shown in Table 3, compounds **4aa**, **4bb**, **5ag**, and **5ah** displayed
387 70−100% control against all the tested weeds at an application rate of 150 g ai/ha. Even at an
388 application rate as low as 37.5 g ai/ha, these compounds still displayed excellent inhibitory
389 activities against all the investigated weeds. For example, compounds **4aa** and **5ag** had almost
390 100% control against *A.r.* and *B.j.*; more than 80% inhibition against *E.p.*, *E.c.*, *A.a.*, and *P.a.*;

and 60% control against *A.t.*, *C.s.*, and *R.a.*. These results indicated that these compounds were nearly as potent as bispyribac. It is worth noting that compounds **4bb** and **5ah** not only displayed >60% inhibition against all the tested weeds but also completely inhibited the growth of *A.t.*, *A.r.*, *E.p.*, and *B.j.* at the lowest application rate of 37.5 g ai/ha.

As previously mentioned, anti-resistance properties are one of the main criteria in AHAS-inhibiting herbicide discovery because commercial AHAS inhibitors are suffering from serious weed resistance problems. To have a better *in vivo* anti-resistance properties, the inhibitor could display equal or high herbicidal activities against sensitive weeds and its resistant weeds. To evaluate whether the target compounds can be potentially developed as anti-resistance herbicides, we further selectively tested the herbicidal activity of representative compounds **4aa** and **4bb** against AHAS herbicide-resistant weeds and the corresponding sensitive weeds (*D. sophia* and *A. arenaria*) at application rates of 0.235−15.0 g ai/ha. Bispyribac, a commercially available AHAS-inhibiting herbicide with the lowest degree of resistance against resistant weeds at present, was used as a positive control. As shown in Table 4, compounds **4aa** and **4bb** exhibited nearly 100% control against AHAS inhibitor-sensitive *D. sophia* and *A. arenaria* and even 90−100% inhibition against AHAS inhibitor-resistant *D. sophia* and *A. arenaria*, indicating their anti-resistance properties were comparable to those of bispyribac at 15.0 g ai/ha. When the spraying dosage was reduced further (3.75−0.94 g ai/ha), compound **4bb** maintained complete inhibition against both sensitive and resistant *D. sophia,* and displayed greater than 92.5% herbicidal activity against both sensitive and resistant *A. arenaria*. Compound **4aa** showed slightly lower herbicidal activity (>85% inhibition against the four tested weeds) than that of compound **4bb**; however,

413 the commercial herbicide bispyribac only moderately inhibited sensitive and resistant weeds
414 at the same application rate. Most promisingly, compounds **4aa** and **4bb** still displayed
415 excellent weed control against both sensitive and resistant *A. arenaria* (>82.5% inhibition)
416 relative to bispyribac at an application rate as low as 0.235 g ai/ha, indicating that **4aa** and
417 **4bb** had better anti-resistance properties than those of bispyribac. These promising findings
418 indicate that compounds **4aa** and **4bb** have great potential to be developed as new lead
419 compounds to combat weeds with resistance to commercial AHAS-inhibiting herbicides.
420 Additional structural optimization and field trial experiments of compounds **4aa** and **4bb** are
421 ongoing.
422
423 **Supporting Information**
424 Detailed information about the single-crystal data of **4bb** (Table S1), comparison of the
425 experimental pK_i and calculated pK_i values (Table S2), inhibition curves for
426 compounds **4aa** and **4bb** against *At*AHAS (Figure S1), HRMS data for compounds **4aa** and
427 **4bb** (Figure S2), binding energy calculation, physical and spectral data of target compounds
428 **4aa**−**bb** and **5aa**−**ah**. This material is available free of charge via the Internet at
429 http://pubs.acs.org.
430
431 **Acknowledgment**
432 We thank Prof. Jie Chen and her research group at Zhejiang Research Institute of Chemical
433 Industry for their help with screening for herbicidal activity. This research was supported by

the National Key R&D Program (2017YFD0200507) and the National Natural Science Foundation of China (No. 21332004).

Notes

The authors declare no competing financial interest.

REFERENCES

(1) Ruegg, W. T.; Quadranti, M.; Zoschke, A., Herbicide research and development: challenges and opportunities. *Weed Res.* **2007**, *47*, 271−275.

(2) Alberto, D.; Serra, A. A.; Sulmon, C.; Gouesbet, G.; Couee, I., Herbicide-related signaling in plants reveals novel insights for herbicide use strategies, environmental risk assessment and global change assessment challenges. *Sci. Total Environ.* **2016**, *569*, 1618−1628.

(3) Duke, S. O., Why have no new herbicide modes of action appeared in recent years?. *Pest Manag. Sci.* **2012**, *68*, 505−512.

(4) Duggleby, R. G.; Pang, S. S., Acetohydroxyacid synthase. *J. Biochem. Mol. Biol.* **2000**, *33*, 1−36.

(5) Green, J. M., Current state of herbicides in herbicide-resistant crops. *Pest. Manag. Sci.* **2014**, *70*, 1351−1357.

(6) Garcia, M. D.; Nouwens, A.; Lonhienne, T. G.; Guddat, L. W., Comprehensive understanding of acetohydroxyacid synthase inhibition by different herbicide families. *Proc. Natl. Acad. Sci.* **2017**, *114*, 1091−1100.

(7) Garcia, M. D.; Wang, J. G.; Lonhienne, T.; Guddat, L. W., Crystal structure of plant acetohydroxyacid synthase, the target for several commercial herbicides. *Febs. J.* **2017**, *284*, 2037-2051

(8) Duggleby, R. G.; McCourt, J. A.; Guddat, L. W., Structure and mechanism of inhibition of plant acetohydroxyacid synthase. *Plant Physiol. Biochem.* **2008**, *46*, 309-24.

(9) Powles, S., Global herbicide resistance challenge. *Pest Manag. Sci.* **2014**, *70*, 1305−1305.

(10) Green, J. M.; Owen, M. D. K., Herbicide-resistant crops: utilities and limitations for herbicide-resistant weed management. *J. Agric. Food. Chem.* **2011**, *59*, 5819−5829.

(11) Burgos, N. R.; Tranel, P. J.; Streibig, J. C.; Davis, V. M.; Shaner, D.; Norsworthy, J. K.; Ritz, C., Review: Confirmation of resistance to herbicides and evaluation of resistance levels. *Weed Sci.* **2013**, *61*, 4−20.

(12) Heap, I. The International Survey of Herbicide-Resistant Weeds. www.weedscience.org (accessed January 11, 2018).

(13) Pandolfo, C. E.; Presotto, A.; Moreno, F.; Dossou, I.; Migasso, J. P.; Sakima, E.; Cantamutto, M., Broad resistance to acetohydroxyacid synthase-inhibiting herbicides in feral radish (*Raphanus sativus L.*) populations from Argentina. *Pest Manag. Sci.* **2016**, *72*, 354−361.

(14) Beckie, H. J.; Warwick, S. I.; Sauder, C. A.; Lozinski, C.; Shirriff, S., Occurrence and molecular characterization of acetolactate synthase (ALS) inhibitor-resistant *Kochia* (*Kochia scoparia*) in western Canada. *Weed Technol.* **2011**, *25*, 170−175.

(15) Tranel, P. J.; Riggins, C. W.; Bell, M. S.; Hager, A. G., Herbicide resistances in *Amaranthus tuberculatus*: a call for new options. *J. Agric. Food Chem.* **2011**, *59*, 5808−5812.

(16) Cui, H. L.; Zhang, C. X.; Zhang, H. J.; Liu, X.; Liu, Y.; Wang, G. Q.; Huang, H. J.; Wei, S. H., Confirmation of flixweed (*Descurainia sophia*) resistance to tribenuron in China. *Weed Sci.* **2008**, *56*, 775−779.

(17) Cui, H. L.; Zhang, C. X.; Wei, S. H.; Zhang, H. J.; Li, X. J.; Zhang, Y. Q.; Wang, G. Q., Acetolactate synthase gene proline (197) mutations confer tribenuron-methyl resistance in flixweed (*Descurainia sophia*) populations from China. *Weed Sci.* **2011**, *59*, 376−379.

(18) Cui, H. L.; Li, X.; Wang, G.; Wang, J.; Wei, S.; Cao, H., Acetolactate synthase proline (197) mutations confer tribenuron-methyl resistance in *Capsella bursa-pastoris* populations from China. *Pestic. Biochem. Physiol.* **2012**, *102*, 229−232.

(19) Wang, J. G.; Tan, H. Z.; Li, Y. H.; Ma, Y.; Li, Z. M.; Guddat, L. W., Chemical synthesis, *in vitro* acetohydroxyacid synthase (AHAS) inhibition, herbicidal activity, and computational studies of isatin derivatives. *J. Agric. Food Chem.* **2011,** *59*, 9892−9900.

(20) Wang, J. G.; Xiao, Y. J.; Li, Y. H.; Ma, Y.; Li, Z. M., Identification of some novel AHAS inhibitors via molecular docking and virtual screening approach. *Bioorg. Med. Chem.* **2007**, *15*, 374−80.

(21) Shang, J.; Wang, W. M.; Li, Y. H.; Song, H. B.; Li, Z. M.; Wang, J. G., Synthesis, crystal structure, *in vitro* acetohydroxyacid synthase inhibition, *in vivo* herbicidal activity, and 3D−QSAR of new asymmetric aryl disulfides. *J. Agric. Food Chem.* **2012**, *60*, 8286−8293.

(22) Li, Y. X.; Luo, Y. P.; Xi, Z.; Niu, C. W.; He, Y. Z.; Yang, G. F., Design and syntheses of novel phthalazin-1(2H)-one derivatives as acetohydroxyacid synthase inhibitors. *J. Agric. Food Chem.* **2006**, *54*, 9135−9139.

(23) Lu, W.; Baig, I. A.; Sun, H. J.; Cui, C. J.; Guo, R.; Jung, I. P.; Wang, D.; Dong, M.; Yoon, M. Y.; Wang, J. G., Synthesis, crystal structure and biological evaluation of substituted quinazolinone benzoates as novel antituberculosis agents targeting acetohydroxyacid synthase. *Eur. J. Med. Chem.* **2015**, *94*, 298-305.

(24) Li, Z. S.; Wang, W. M.; Lu, W.; Niu, C. W.; Li, Y. H.; Li, Z. M.; Wang, J. G., Synthesis and biological evaluation of nonsymmetrical aromatic disulfides as novel inhibitors of acetohydroxyacid synthase. *Bioorg. Med. Chem. Lett.* **2013**, *23*, 3723-3727.

(25) He, Y. Z.; Li, Y. X.; Zhu, X. L.; Xi, Z.; Niu, C. W.; Wan, J.; Zhang, L.; Yang, G. F., Rational design based on bioactive conformation analysis of pyrimidinylbenzoates as acetohydroxyacid synthase inhibitors by integrating molecular docking, CoMFA, CoMSIA, and DFT calculations. *J. Chem. Inf .Model.* **2007**, *47*, 2335−2344.

(26) Ji, F. Q.; Niu, C. W.; Chen, C. N.; Chen, Q.; Yang, G. F.; Xi, Z.; Zhan, C. G., Computational design and discovery of conformationally flexible inhibitors of acetohydroxyacid synthase to overcome drug resistance associated with the W586L mutation. *ChemMedChem* **2008**, *3*, 1203−1206.

(27) Chen, C. N.; Lv, L. L.; Ji, F. Q.; Chen, Q.; Xu, H.; Niu, C. W.; Xi, Z.; Yang, G. F., Design and synthesis of *N*-2,6-difluorophenyl-5-methoxyl-1,2,4-triazolo[1,5-*a*] -pyrimidine-2-sulfonamide as acetohydroxyacid synthase inhibitor. *Bioorg. Med. Chem.* **2009**, *17*, 3011−3017.

(28) Chen, C. N.; Chen, Q.; Liu, Y. C.; Zhu, X. L.; Niu, C. W.; Xi, Z.; Yang, G. F., Syntheses and herbicidal activity of new triazolopyrimidine-2-sulfonamides as acetohydroxyacid synthase inhibitor. *Bioorg. Med. Chem.* **2010**, *18*, 4897−4904.

(29) Liu, Y. C.; Qu, R. Y.; Chen, Q.; Yang, J. F.; Niu, C. W.; Zhen, X.; Yang, G. F., Triazolopyrimidines as a new herbicidal lead for combating weed resistance associated with acetohydroxyacid synthase mutation. *J. Agric. Food Chem.* **2016**, *64*, 4845−4857.

(30) Qu, R. Y.; Yang, J. F.; Liu, Y. C.; Chen, Q.; Hao, G. F.; Niu, C. W.; Xi, Z.; Yang, G. F., Computational design of novel inhibitors to overcome weed resistance associated with acetohydroxyacid synthase (AHAS) P197L Mutant. *Pest Manag. Sci.* **2017**, *73*, 1373−1381.

(31) Qu, R. Y.; Yang, J. F.; Devendar, P.; Kang, W. M.; Liu, Y. C.; Chen, Q.; Niu, C. W.; Xi, Z.; Yang, G. F., Discovery of new 2-[(4,6-dimethoxy-1,3,5-triazin -2-yl)oxy] -6-(substitutedphenoxy)benzoic acids as flexible inhibitors of *Arabidopsis thaliana* acetohydroxyacid synthase and its P197L mutant. *J. Agric. Food Chem.* **2017**, *65*, 11170−11178.

(32) Lamberth, C., Agrochemical lead optimization by scaffold hopping. *Pest Manag. Sci.* **2018**, *74*, 282−292

(33) Ujváry, I., Extended summary: BIOSTER—a database of structurally analogous compounds. *Pest Manag. Sci.* **1997**, *51*, 92−95.

(34) Hu, Y.; Stumpfe, D.; Bajorath, J., Recent advances in scaffold hopping. *J. Med. Chem.* **2017**, *60*, 1238−1246.

(35) Böhm, H. J.; Flohr, A.; Stahl, M., Scaffold hopping. *Drug Discovery Today: Technol.* **2004**, *1*, 217−224.

543 (36) Odell, L. R.; Abdel-Hamid, M. K.; Hill, T. A.; Chau, N.; Young, K. A.; Deane, F. M.;
544 Sakoff, J. A.; Andersson, S.; Daniel, J. A.; Robinson, P. J.; McCluskey, A., Pyrimidine-based
545 inhibitors of dynamin I GTPase activity: competitive inhibition at the pleckstrin homology
546 domain. *J. Med. Chem.* **2017**, *60*, 349−361.
547 (37) Lagoja, I. M., Pyrimidine as constituent of natural biologically active compounds.
548 *Chem. Biodivers.* **2005**, *2*, 1−50.
549 (38) Gerwick, B. C.; Subramanian, M. V.; Loney-Gallant, V. I.; Chandler, D. P., Mechanism
550 of action of the 1,2,4-triazolo[1, 5-*a*]pyrimidines. *Pest Manag. Sci.* **1990**, *29*, 357−364.
551 (39) McCourt, J. A.; Pang, S. S.; King-Scott, J.; Guddat, L. W.; Duggleby, R. G.,
552 Herbicide-binding sites revealed in the structure of plant acetohydroxyacid synthase. *Proc.*
553 *Natl. Acad. Sci.* **2006**, *103*, 569-573.
554 (40) Liu, Y. C.; Huang, Z. Y.; Chen, Q.; Yang, G. F., Efficient synthesis of functionalized
555 6-arylsalicylates via microwave-promoted Suzuki cross-coupling reaction. *Tetrahedron*
556 **2013**, *69*, 9025−9032.
557 (41) Qu, R. Y.; Liu, Y. C.; Wu, Q. Y.; Chen, Q.; Yang, G. F., An efficient method for
558 syntheses of functionalized 6-bulkysubstituted salicylates under microwave irradiation.
559 *Tetrahedron* **2015**, *71*, 8123−8130.
560 (42) Qu, R. Y.; Chen, N.; Liu, Y. C.; Chen, Q.; Yang, G. F., An Efficient Synthesis of
561 functionalized 6-Arylsubstituted salicylates via microwave irradiation. *Chin. J. Org. Chem.*
562 **2017**, *37*, 1266−1272.
563 (43) The Cambridge Crystallographic Data Centre (CCDC). https://www.ccdc.cam.ac.uk/
564 (accessed June 07, 2017).

565 (44) Sitkoff, D.; Sharp, K. A.; Honig, B., Accurate calculation of hydration free energies
566 using macroscopic solvent models. *J. Phys. Chem.* **1994**, *98*, 1978−1988.
567 (45) Wang, D. W.; Lin, H. Y.; He, B.; Wu, F. X.; Chen, T.; Chen, Q.; Yang, W. C.; Yang,
568 G. F., An efficient one-pot synthesis of 2-(aryloxyacetyl)cyclohexane-1,3-diones as
569 herbicidal 4-hydroxyphenylpyruvate dioxygenase inhibitors. *J. Agric. Food Chem.* **2016**,
570 *64*, 8986−8993.
571 (46) Rautio, J.; Kumpulainen, H.; Heimbach, T.; Oliyai, R.; Oh, D.; Jarvinen, T.; Savolainen,
572 J., Prodrugs: design and clinical applications. *Nat*. *Rev*. *Drug Discov*. **2008**, *7*, 255−270.
573
574

FIGURE CAPTIONS:

Figure 1. Design of the target compounds **4** and **5** and simulated binding modes of representative compounds **A** and **4aa** with *At*AHAS. The key residues surrounding the active site are shown as blue sticks, and the structure of representative compounds **A** and **4aa** are shown in green and pink, respectively.

Figure 2. Synthetic routes of compounds **4aa**–**bb** and **5aa**–**ah**. Reagents and conditions: (a) 30% aqueous H_2O_2, $Na_2WO_4 \cdot 2H_2O$, AcOH, 50 °C; (b) K_2CO_3, anhydrous toluene, reflux; (c) 1 N HCl solution; (d) R^3-X (X = I or Br), Cs_2CO_3, DMF, RT; (e) NaOH, THF, RT.

Figure 3. Synthetic routes of key intermediates **3**. Reagents and conditions: Method A: (a) I_2, $Pd(OAc)_2$, $PhI(OAc)_2$, DMF, 100 °C; (b) $R^1B(OH)_2$, $Pd(PPh_3)_4$, K_2CO_3, DME/H_2O, microwave−assisted, 110 °C; (c) BBr_3, anhydrous CH_2Cl_2, −78 °C. Method B: (d) CO_2, $KHCO_3$, glycerol, 100 °C; (e) acetone, $SOCl_2$, DME; (f) Tf_2O, Et_3N, CH_2Cl_2; (g) $R^1B(OH)_2$, $Pd(PPh_3)_4$, $NaHCO_3$, DME/H_2O, microwave−assisted, 110 °C; (h) KOH, THF/H_2O, reflux; (i) concentrated HCl.

Figure 4. X-ray crystal structure of compound **4bb**.

Figure 5. Simulated binding mode of compounds **4aa**, **4ax**, **4az** and **4bb** with *At*AHAS. The key residues and molecules in the active site are shown as blue sticks. The hydrogen bond distance (Å) is shown as black lines. (A) Binding mode of **4aa** with *At*AHAS. (B) Binding mode of **4ax** with *At*AHAS. The red arrow represents the direction of its conformational excursion compared with that of **4bb**. (C) Binding mode of **4az** with *At*AHAS. The pink circle covering D376 indicates the electrostatic repulsion between this residue and compound **4az**. (D) Binding mode of **4bb** with *At*AHAS.

597 **Figure 6**. Correlation between the experimental and calculated *At*AHAS inhibitory activities
598 (pK_i).

599 **Figure 7**. (A) CoMFA map for electrostatic contribution. Compound **4bb** is shown inside the
600 field. Blue contours mean the increase of positive charge, which will promote the activity; on
601 the contrary, the activity is enhanced if the negative charges are increased in the red contour
602 areas. (B) CoMFA prediction of steric contribution. Compound **4bb** is shown inside the graph.
603 The yellow map represents the sterically disadvantageous areas where bulkier groups are
604 beneficial for the enzyme inhibitory activity, and the green area means the opposite. (C)
605 Alignments of 21 compounds of the training set.

Table 1. Chemical Structure, Herbicidal Activity[a] and *At*AHAS Inhibitory Activities of Compounds **4aa−4bb** and **5aa−5ah**

compd.	R^1	R^2	R^3	% inhibition						*At*AHAS inhibition
				B.j.[b]	*C.s.*	*R.a.*	*A.a.*	*P.f.*	*P.a.*	K_i (μM)[c]
4aa	phenyl	Me	H	100	80	80	90	90	90	0.09
4ab	pyridin-3-yl	Me	H	100	0	0	30	50	30	5.31
4ac	6-F-pyridin-3-yl	Me	H	80	30	50	80	60	30	30.90
4ad	6-Cl-pyridin-3-yl	Me	H	80	0	0	0	0	0	9.89
4ae	5-Me-pyridin-3-yl	Me	H	0	0	0	0	0	0	49.80
4af	5-Cl-pyridin-3-yl	Me	H	80	0	0	30	0	0	4.52
4ag	pyrimidin-5-yl	Me	H	30	0	0	0	0	0	705.00
4ah	2-OMe-pyrimidin-5-y	Me	H	0	0	0	0	0	0	59.70
4ai	furan-2-yl	Me	H	60	0	60	50	0	0	0.66
4aj	furan-3-yl	Me	H	70	0	50	70	0	0	0.51
4ak	3,5-diMeisoxazol-4-yl	Me	H	50	0	0	70	30	30	3.78
4al	naphthalen-2-yl	Me	H	40	0	0	50	30	30	0.25
4am	4-Me-phenyl	Me	H	100	60	80	80	80	80	0.18
4an	4-OMe-phenyl	Me	H	40	30	30	50	40	50	1.54
4ao	4-NO_2-phenyl	Me	H	50	30	30	50	30	30	2.73
4ap	2-F-phenyl	Me	H	40	0	40	50	0	0	2.07
4aq	3-F-phenyl	Me	H	70	70	70	70	70	80	2.15
4ar	4-F-phenyl	Me	H	80	30	50	50	30	0	0.67
4as	2-Cl-phenyl	Me	H	80	30	30	70	0	40	2.91
4at	3-Cl-phenyl	Me	H	100	50	30	70	0	0	4.03
4au	4-Cl-phenyl	Me	H	100	50	30	70	40	40	0.20
4av	4-Br-phenyl	Me	H	80	0	60	70	30	30	0.41
4aw	3.5-diF-phenyl	Me	H	100	80	50	80	50	40	7.28
4ax	phenyl	OMe	H	0	0	0	30	0	0	26.80
4ay	4-Cl-phenyl	OMe	H	0	0	0	0	0	0	39.10
4az	phenyl	F	H	0	0	0	0	0	0	663.00
4ba	phenyl	Cl	H	60	0	0	0	0	0	>1000
4bb	phenyl	H	H	100	80	85	100	100	90	0.02
5aa	phenyl	Me	Me	50	30	50	40	40	0	–[d]
5ab	phenyl	Me	Et	30	0	30	0	30	0	–
5ac	phenyl	H	Me	70	50	60	30	30	30	–
5ad	phenyl	Me	CH_2COOMe	0	0	0	0	0	0	–
5ae	phenyl	Me	CH_2COOEt	0	0	0	0	0	0	–
5af	phenyl	Me	$CHCH_3COOMe$	0	0	0	0	0	0	–
5ag	phenyl	Me	Na	100	80	80	80	80	80	–
5ah	phenyl	H	Na	100	75	80	95	85	90	–
flumetsulam				90	85	85	60	50	60	0.38
bispyribac				100	80	85	90	80	95	0.54

[a]Herbicidal activity was tested at a rate of 150 g ai/ha. [b]Abbreviations: *B.j.*, *Brassica juncea*; *C.s.*, *Chenopodium serotinum; R.a.*, *Rumex acetosa*; *A.a.*, *Alopecurus aequalis*; *P.f.*, *Polypogon fugax*; *P.a.*, *Poa annua.* [c]Inhibition constant of the enzymatic reaction. [d]– = no test.

Table 2 Binding Free Energies of **4aa**, **4ax**, **4az**, and **4bb**

Compd.	ΔE_{ELE} kcal mol^{-1}	ΔE_{VDW} kcal mol^{-1}	ΔE_{GAS} kcal mol^{-1}	ΔE_{PBSOL} kcal mol^{-1}	ΔE_{PBTOT} kcal mol^{-1}	$-T\Delta S$ kcal mol^{-1}	ΔG_{cal}[a] kcal mol^{-1}
4aa	−66.39	−58.19	−124.58	83.20	−41.38	22.70	−18.69
4ax	−49.89	−60.42	−110.31	71.13	−39.19	22.88	−16.31
4az	−55.10	−56.98	−112.09	79.22	−32.87	19.49	−13.38
4bb	−66.85	−56.38	−123.23	84.24	−38.99	18.62	−20.37

[a]Results were determined by MM/PBSA calculation.

Table 3. Herbicidal Activity of Compounds **4aa**, **4bb**, **5ag**, and **5ah**

compd.	dosage (g ai/ha)	% inhibition										
		A.t.[a]	*A.r.*	*E.p.*	*D.s.*	*E.c.*	*B.j.*	*C.s.*	*R.a.*	*A.a.*	*P.f.*	*P.a.*
4aa	150	80	100	100	70	90	100	80	80	90	90	90
	75.0	70	100	95	60	85	100	80	70	90	80	90
	37.5	60	100	90	50	80	100	70	65	80	60	80
4bb	150	100	100	100	80	90	100	80	85	100	100	90
	75.0	100	100	100	70	85	100	70	70	90	80	90
	37.5	100	100	100	50	80	100	60	60	80	70	80
5ag	150	80	100	100	70	90	100	80	80	80	80	80
	75.0	70	100	90	60	85	100	70	70	90	60	90
	37.5	60	100	85	40	80	100	60	60	80	50	80
5ah	150	100	100	100	85	90	100	75	80	95	85	90
	75.0	100	100	100	80	85	100	70	70	90	85	90
	37.5	100	100	90	70	80	100	60	60	80	75	80
bispyribac	150	100	100	100	70	90	100	80	85	90	80	95
	75.0	100	100	90	60	85	100	75	80	85	70	90
	37.5	100	100	80	50	80	100	70	70	80	60	80

[a]Abbreviations: *A.t.*, *Abutilon theophrasti*; *A.r.*, *Amaranthus retroflexus*; *E.p.*, *Eclipta prostrata*; *D.s.*, *Digitaria sanguinalis*; *E.c.*, *Echinochloa crusgalli*; *B.j.*, *Brassica juncea*; *C.s.*, *Chenopodium serotinum; R.a.*, *Rumex acetosa*; *A.a.*, *Alopecurus aequalis*; *P.f.*, *Polypogon fugax*; *P.a.*, *Poa annua*.

Table 4. Herbicidal Activity Comparison of Representative Compounds **4aa** and **4bb** against AHAS Inhibitor-Sensitive and AHAS Inhibitor-Resistant Weeds

compd.	dosage (g ai/ha)[a]	% inhibition			
		Sensitive *D. sophia*[b]	Resistant *D. sophia*[b]	Sensitive *A. arenaria*[b]	Resistant *A. arenaria*[b]
4aa	15.0	100	90	97.5	98
	3.75	100	90	90	92.5
	0.94	100	85	85	87.5
	0.235	–[c]	–	82.5	82.5
4bb	15.0	100	100	98	99
	3.75	100	100	98	96.5
	0.94	100	100	95	92.5
	0.235	–	–	87.5	92.5
bispyribac	15.0	100	100	95	98
	3.75	90	85	95	95
	0.94	67.5	60	85	80
	0.235	–	–	80	40

[a] 15 g ai/ha = 1 g ai/mu; 3.75 g ai/ha = 1/4 g ai/mu; 0.94 g ai/ha = 1/16 g ai/mu; 0.235 g ai/ha = 1/64 g ai/mu.
[b]Abbreviations: *D. sophia*, *Descurainia sophia*; *A. arenaria*, *Ammannia arenaria*. [c]– = no test.

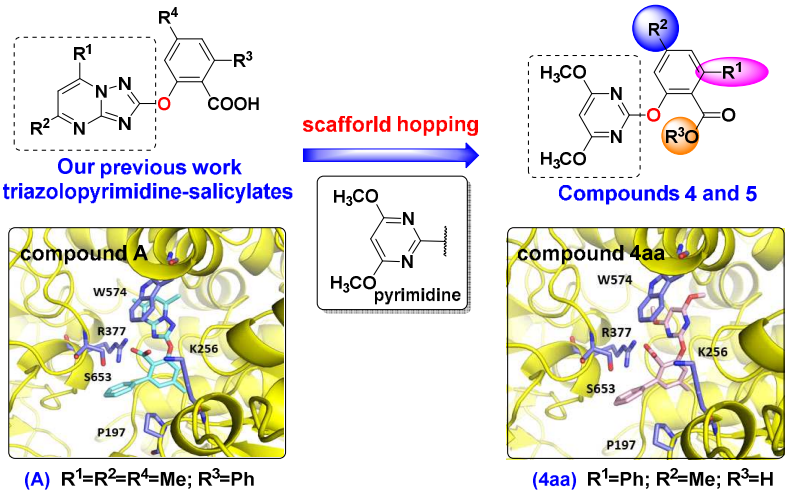
Our previous work
triazolopyrimidine-salicylates
scafforld hopping
pyrimidine
Compounds 4 and 5
compound A
compound 4aa
W574
R377
K256
S653
P197
(A) R1=R2=R4=Me; R3=Ph
(4aa) R1=Ph; R2=Me; R3=H

Figure 1.

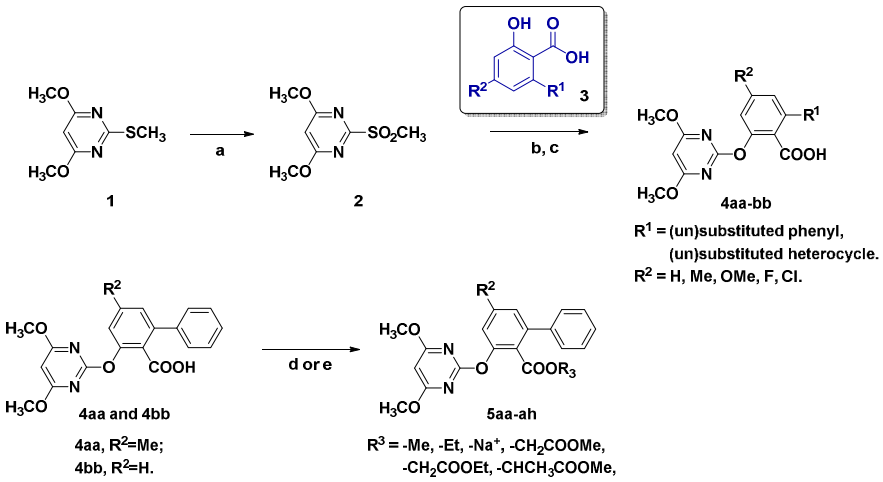
1
a
2
b, c
3
4aa-bb
R1 = (un)substituted phenyl,
(un)substituted heterocycle.
R2 = H, Me, OMe, F, Cl.
4aa and 4bb
4aa, R2=Me;
4bb, R2=H.
d or e
5aa-ah
R3 = -Me, -Et, -Na+, -CH2COOMe,
-CH2COOEt, -CHCH3COOMe,

Figure 2.

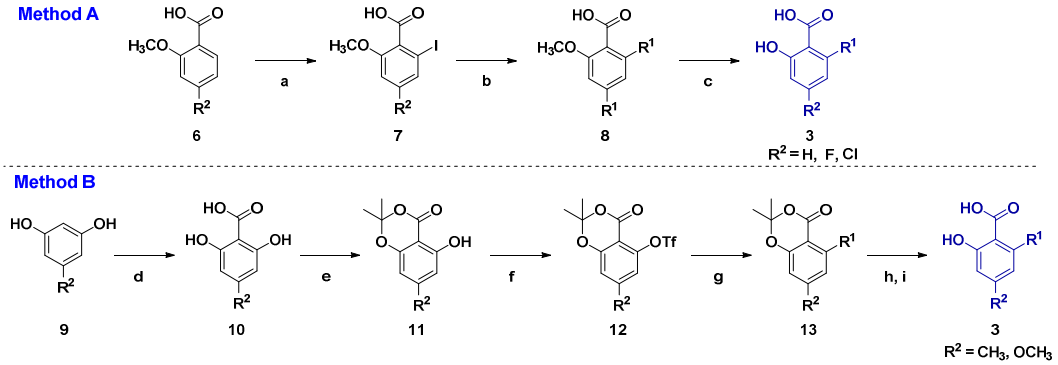
Method A
HO
O
H3CO
R2
6
a
I
7
b
R1
8
c
HO
R1
3
R2 = H, F, Cl
Method B
OH
9
d
10
e
11
f
OTf
12
g
13
h, i
R2 = CH3, OCH3

Figure 3.

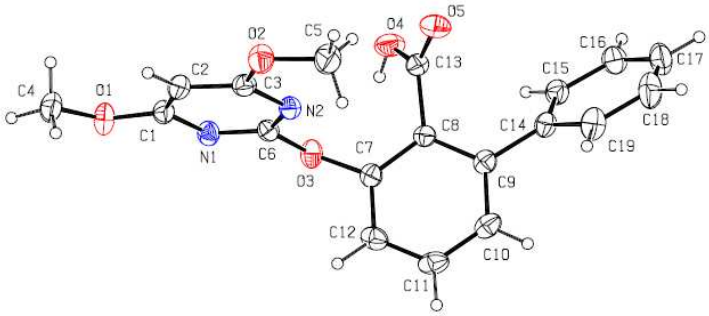
O2
C5
O4
O5
C16
C17
C4
O1
C2
C3
C13
C15
N2
C8
C14
C18
C1
N1
C6
C7
C19
O3
C9
C12
C10
C11

Figure 4.

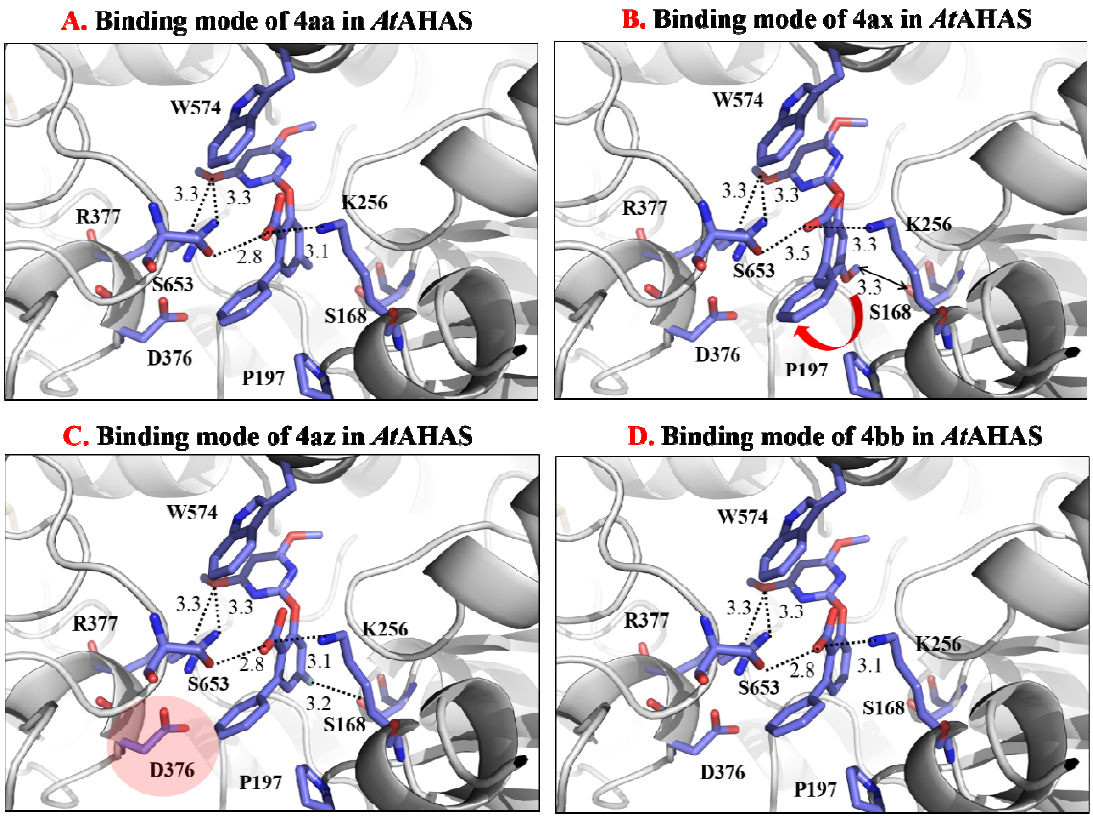
A. Binding mode of 4aa in AtAHAS
W574
R377
K256
S653
S168
D376
P197
3.3
3.3
2.8
3.1
B. Binding mode of 4ax in AtAHAS
W574
R377
K256
S653
S168
D376
P197
3.3
3.3
3.5
3.3
3.3
C. Binding mode of 4az in AtAHAS
W574
R377
K256
S653
S168
D376
P197
3.3
3.3
2.8
3.1
3.2
D. Binding mode of 4bb in AtAHAS
W574
R377
K256
S653
S168
D376
P197
3.3
3.3
2.8
3.1

Figure 5.

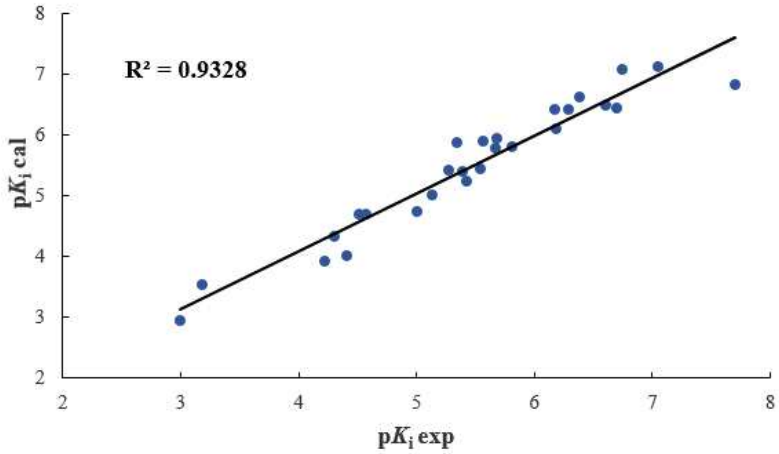

Figure 6.

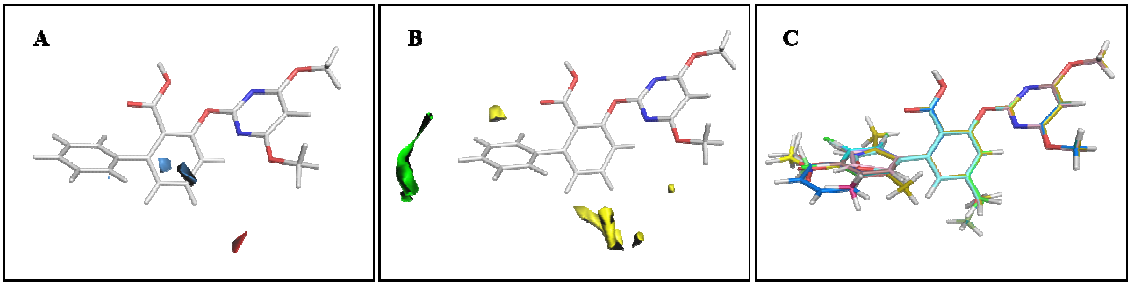

Figure 7.

Table of Contents Graphic